THE DYNAMICS OF GEORGE VI ICE SHELF

By M. R. PEARSON *and* I. H. ROSE

ABSTRACT. Experiments aimed at understanding the factors which affect mass flux at the bottom surface of an ice shelf have been made. Surface strain-rates were observed together with net balance at a number of points. Flow lines were determined from satellite imagery used together with survey measurements. Ice thicknesses were measured by airborne radio echo sounding. Bottom-flux profiles measured across the direction of flow allowed discrete ice streams within the ice shelf to be detected. In one area, an ice regime analogous to that of a consuming plate boundary in contemporary plate-tectonic theory was found.

MASS flux at the bottom surface of the ice shelves is probably the least-known term in the mass balance of Antarctica. Earlier work by the British Antarctic Survey (Thomas and Coslett, 1970) suggested that bottom flux might embrace the critical difference between a positive and a negative net balance for the whole Antarctic ice sheet. Experiments aimed at understanding the factors which affect mass flux at the bottom surface of an ice shelf have now been made.

While most Antarctic ice shelves terminate in a single ice front, the ice shelf in George VI Sound (Fig. 1) is confined between parallel flanks of land ice and it apparently flows towards an ice front at each end of the sound. It is 500 km. long, 20–60 km. wide and it bridges the gap between Alexander Island and Palmer Land. Radio echo sounding (Swithinbank, 1968) has established that it is afloat, that it varies in thickness from 100 m. to about 500 m. and that its thickest part lies close to its southern end. There is extensive summer surface melting on an area of the ice shelf between Ablation Point and Two Step Cliffs. This melting has been attributed to the heat absorption of rock dust blown on to the ice shelf from sedimentary rocks forming the east coast of Alexander Island (Wager, 1972), but it is evidently also due to melt water flowing from nunataks on to the ice shelf.

Mass flux at both top and bottom surfaces is significant in the net mass balance of an ice shelf but it can only be measured directly at the top surface. Measurements of ice thickness, snow accumulation, density, velocity and the horizontal components of surface deformation have been used to calculate the mass flux at a series of points on the bottom surface of the ice shelf.

SURVEY METHOD

It was known from radio echo sounding (Swithinbank, 1968) that the thickest part of the ice shelf is near long. 70°W. From this it was concluded that the direction of flow was probably from an ice divide in that vicinity towards the ice fronts at both ends of the sound. However, oblique air photographs taken in 1966 indicated that the ice might be flowing not along but across the sound in lat. 71°S. A subdued ridge marking the confluence of two ice streams was seen to run from Gurney Point across the sound in a westerly direction to the southern end of the Ablation Point massif. Survey markers set on the ice shelf 15 km. south of Ablation Point were found to have moved west during a 17 day period of observation in 1968 (personal communication from A. C. Wager).

In order to investigate the area more fully, lines of survey markers were set out from a rock ridge in lat. 70°18′S., long. 69°04′W. to Carse Point, from Fossil Bluff across the ice shelf to a promontory in lat. 71°18′S., and from Coal Nunatak to Buttress Nunataks. Each marker or snow stake consisted of a 4 m. length of aluminium tubing of 25 mm. outside diameter and 2 mm. wall thickness drilled into the ice to a depth of between 1·5 and 2·0 m. Because of extensive melt in the latitude of Fossil Bluff, most of the stakes on the middle line were lost and no useful results were obtained. The Coal Nunatak profile (Fig. 2) consisted of an almost

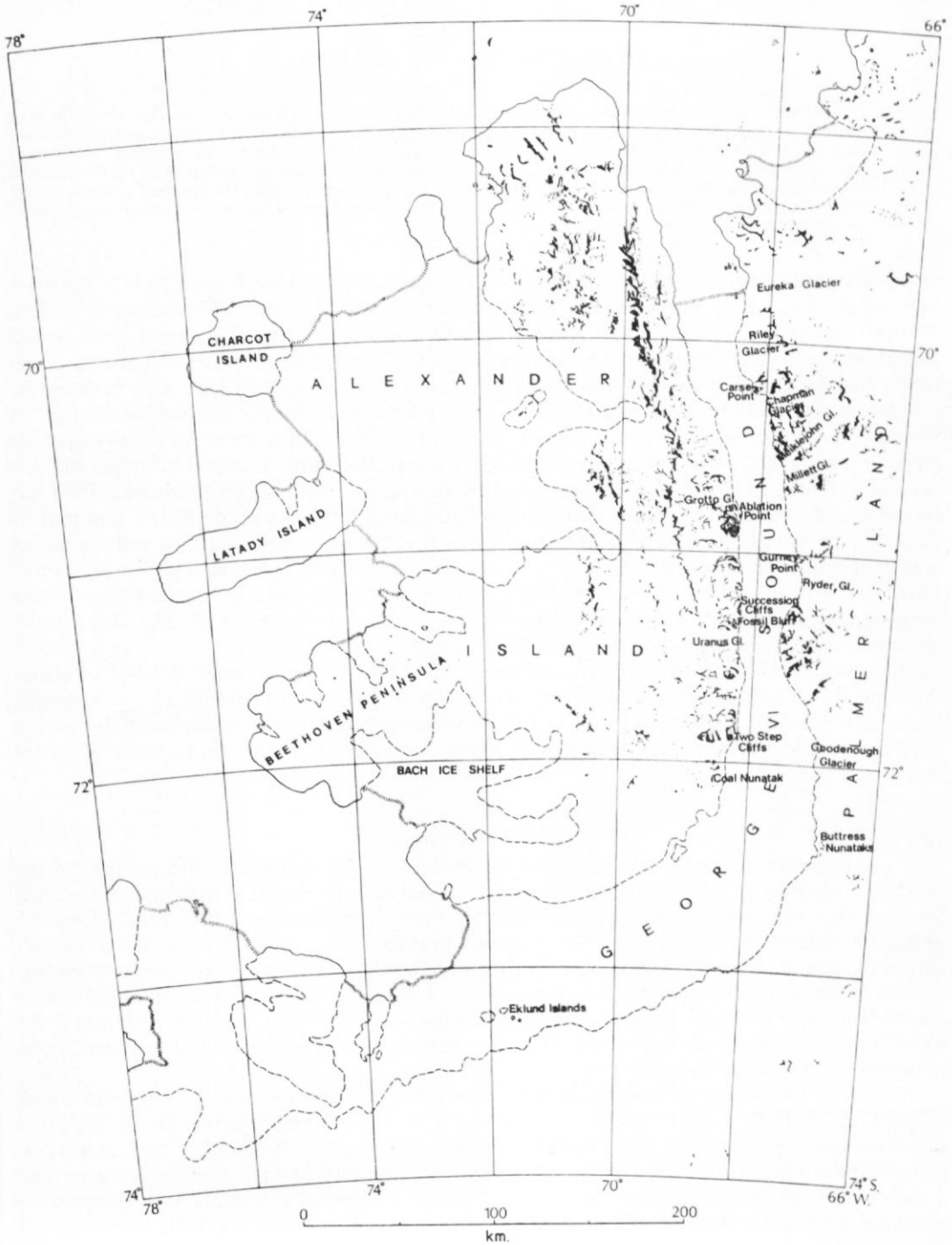

Fig. 1. Map of George VI Sound with place-names used in the text.

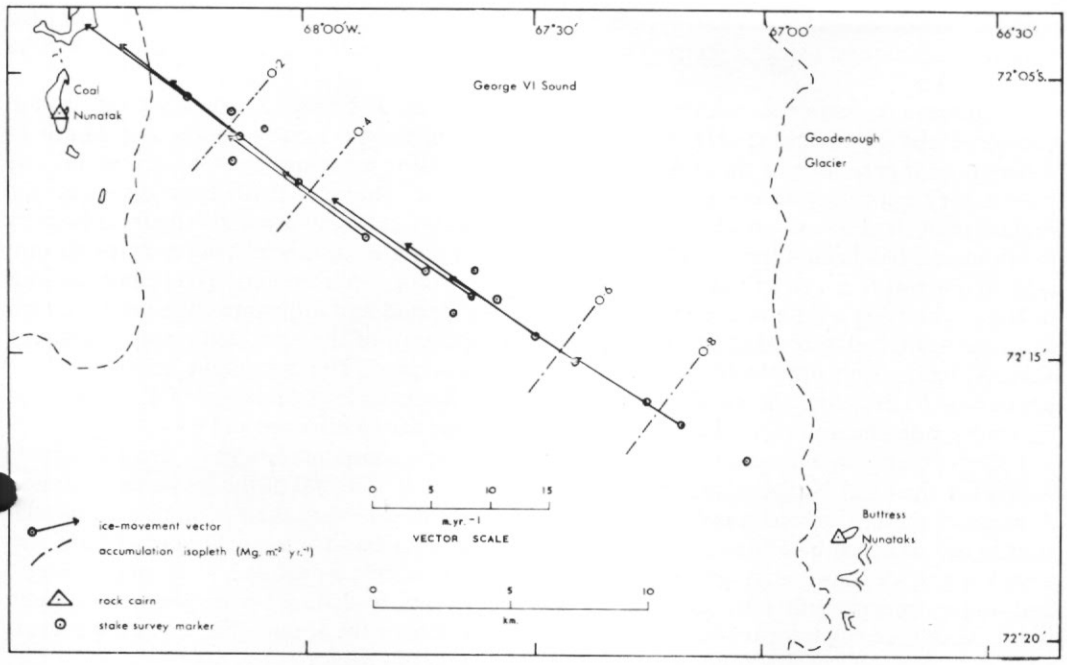

Fig. 2. Ice-movement vectors and snow-accumulation isopleths on the Coal Nunatak profile.

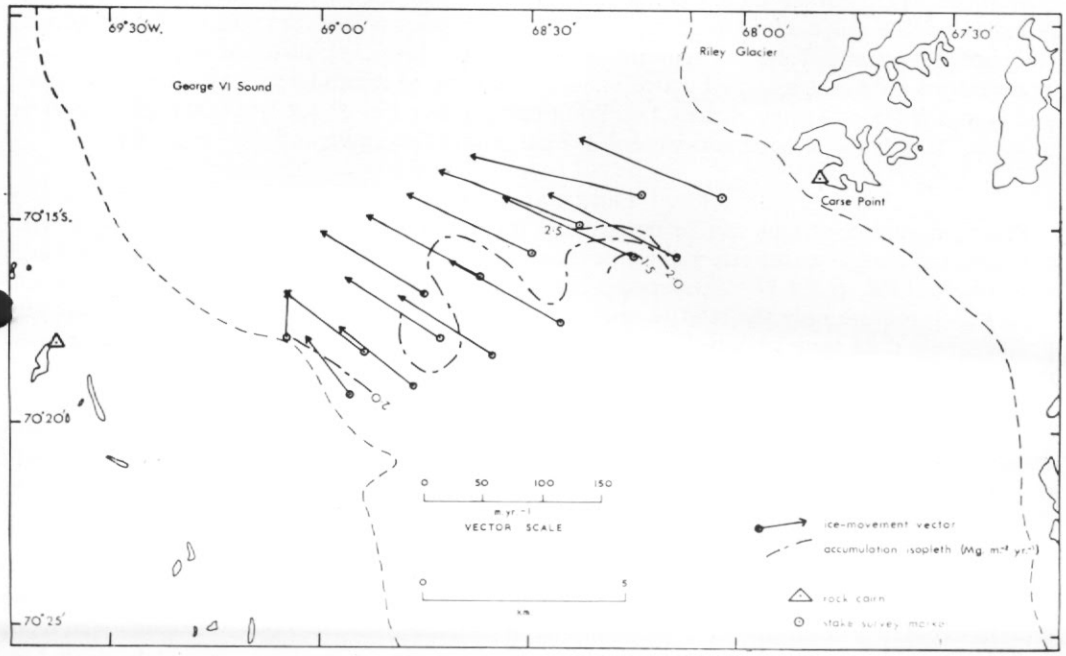

Fig. 3. Ice-movement vectors and snow-accumulation isopleths on the Carse Point profile.

straight line of stakes. It was surveyed in October 1971 and again in October 1972 by standard traverse techniques using a Zeiss Th-2 single-second self-indexing theodolite and MRA3 tellurometers.

All glaciers consist of ice which is continuously deforming. Since each survey took days to complete, the observations refer to different times during the survey period and hence to different configurations of the stake pattern. A computation using unadjusted data would give only a very approximate result. Swithinbank (1958) and Thomas (1970) have discussed the reduction of data to one epoch in time and for the purposes of this work the method used by Swithinbank has been adopted. This assumes that angles and distances deform at a constant rate. While this is not strictly true, it represents a satisfactory approximation over short periods of time. Choosing a date in the middle of the survey period and adjusting each measurement to its probable value on that day by applying a proportion of the total deformation between surveys, values appropriate to the epoch day were obtained. The maximum departure from epoch was 10 days and the mean departure 3 days with a standard deviation of 2·9 days. The maximum adjustment involved was 0·02 per cent of a measured distance and 0·01° of arc.

Using a cairn on Buttress Nunataks as origin, survey computations gave two coordinate values for the Coal Nunatak cairn which differed by about 1/70,000 of the traversed distance. A mean of these positions was taken and all stake coordinates were then re-computed in relation to the accepted positions of the cairns. Comparison of the stake coordinates of both surveys yielded ice-movement vectors (Fig. 2). Positional uncertainties due to errors in length and angle measurement were assumed to be proportional to distance from the nearest fixed point. Vector errors were therefore greatest in the middle of the sound. The maximum errors were $\pm 1 \cdot 5$ per cent of the length and $\pm 1°$ in the azimuth of a vector.

The other stake system, known as the Carse Point profile, ran across the sound between a rock cairn on Alexander Island and another on Carse Point (Fig. 3). It consisted of a series of triangles and was surveyed by tellurometer trilateration in November 1971 and again in November 1972. Survey data were reduced to epoch in the manner adopted for the Coal Nunatak profile, the maximum departure from epoch being 6 days, the mean 2·1 days and the standard deviation 1·7 days. Maximum correction to a measured distance was 0·02 per cent. The western cairn was assigned coordinates of 5,000 m. north and 0 m. east of a false origin, and computed coordinates of the Carse Point cairn differed by about 1/65,000 of the traversed distance. Maximum vector errors were $\pm 2 \cdot 7$ per cent of the length and $\pm 1°$ in azimuth.

Principal Strains

Principal surface strains can be determined for any group of three stakes forming a well-conditioned triangle whose size and shape is known on different occasions. Kehle (*in* Zumberge and others, 1960, p. 59–66) developed a series of equations for calculating principal strain-rates which require only the relative coordinates of the stakes as data. On the Coal Nunatak profile, these data were obtained only at two groups of stakes known as strain rosettes, one in the middle of the ice shelf and one on the western side. Each group consisted of three stakes spaced about 120° apart and 1 km. distant from a central stake. The Carse Point profile was set out as a triangular system of stakes in order that a much more complete coverage of strain information would be obtained. 11 stake triangles were chosen and principal strains were calculated for the centre of each triangle. The direction and magnitude of the strain-rates on the Coal Nunatak and Carse Point profiles are shown in Figs. 4 and 5.

Surface Net Balance

The water equivalent of the snow accumulation was deduced from measurements of stake lengths exposed and surface snow densities taken on each visit. Densities were calculated from measurements of the weight and volume of rectilinear snow blocks taken from pits up to 3 m. deep. Three pits were dug on the Coal Nunatak profile and two on the Carse Point profile.

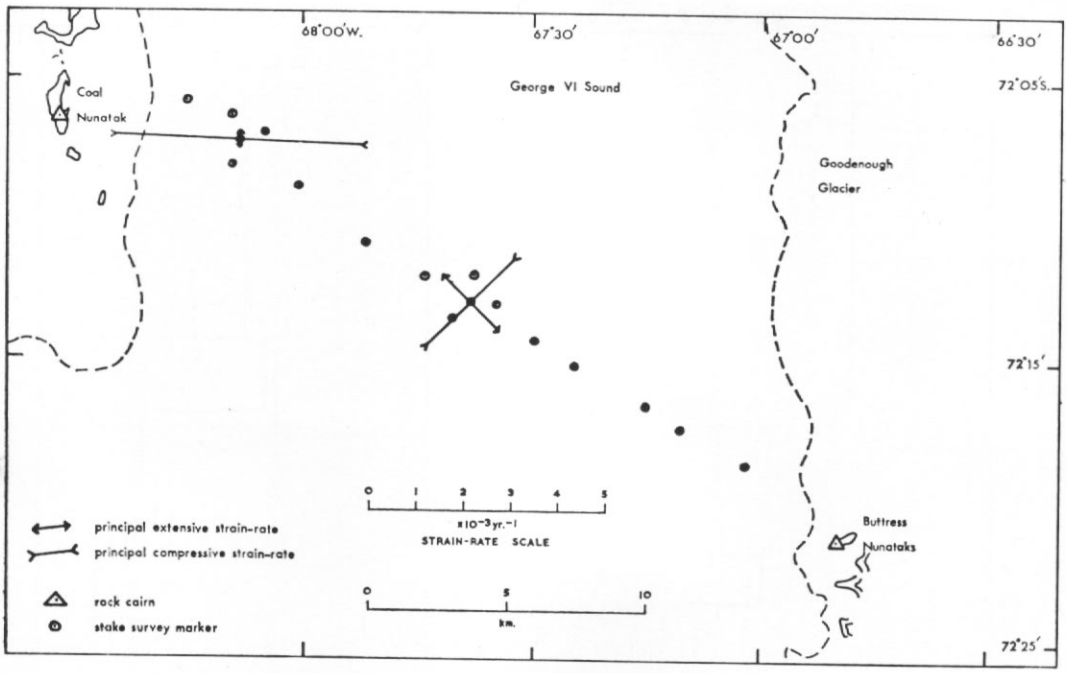

Fig. 4. Principal strain-rates on the Coal Nunatak profile.

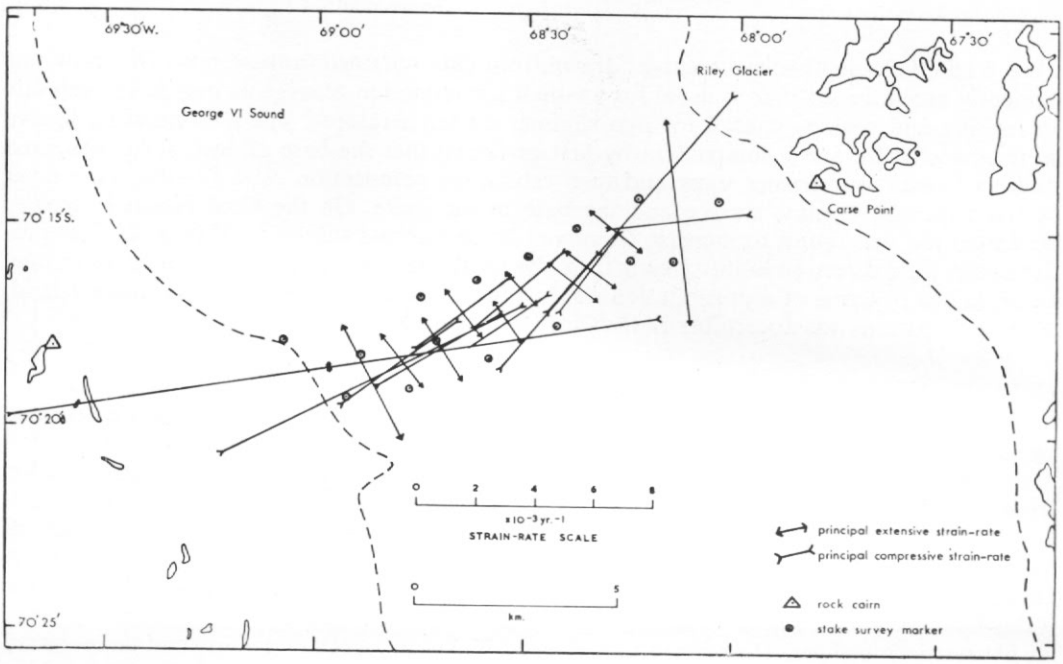

Fig. 5 Principal strain-rates on the Carse Point profile.

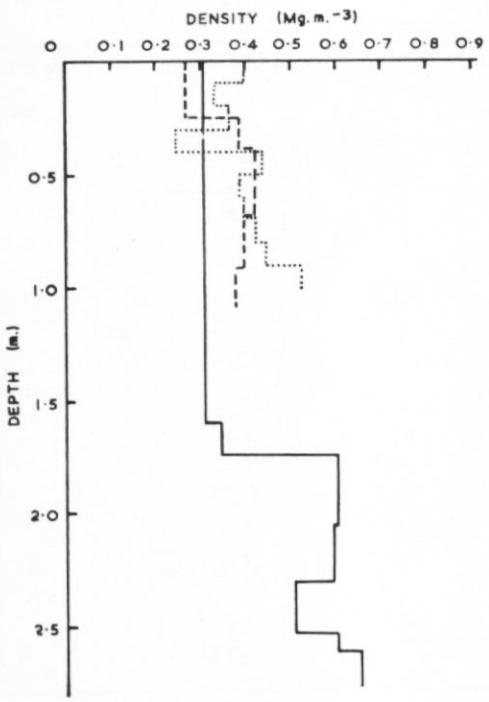

Fig. 6. Depth–density profiles from snow pits on the Coal Nunatak profile. The dotted line indicates results from the middle of the ice shelf, while the solid and dashed lines indicate results from the eastern side.

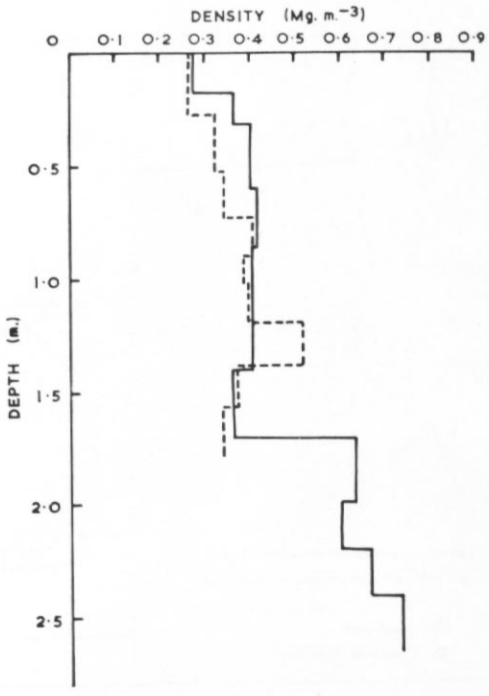

Fig. 7. Depth–density profiles from snow pits on the Carse Point profile. The solid line indicates results from the middle of the ice shelf, while the dashed line indicates results from the western side.

Figs. 6 and 7 are depth–density curves drawn from data obtained in these pits. The snow was evidently much denser than is usual for ice-shelf accumulation areas; this may have been due to melting and soaking caused by high summer air temperatures. The accumulation figures were corrected for snow compaction by first assuming that the base of each stake was fixed relative to the surrounding snow and then estimating compaction rates for the snow layer between the initial snow surface and the base of the stake. On the Coal Nunatak profile, accumulation was found to increase from west to east across the ice shelf (Fig. 2). The predominant wind direction in this area is from the north-west (Wager, 1972) so the pattern may be explained in terms of a precipitation shadow in the lee of south-eastern Alexander Island. No overall pattern was discernible on the Carse Point profile.

Ice-shelf Density

Two different mean densities have been calculated for the ice shelf: one for the area affected by surface melting and another for the ice shelf to the north and south of the melt area.

In May 1973, surface elevations were measured by optical levelling (personal communication from J. F. Bishop) on a line extending 20 km. from apparent sea-level in a tidal lake in lat. 70°52′S., long. 68°20′W. towards Gurney Point. The lake collects melt water that runs off the surrounding rocks in summer, and in winter the surface freezes to a depth of 1–2 m. A continuous record of tidal rise and fall was obtained with a Soviet model GR-38 long-action water-level recorder. Profiles of salinity and temperature were measured by J. F. Bishop using an Electronic Switchgear (London) Limited type MC5 oceanographic salinity and temperature bridge equipped with 100 m. of cable. Fig. 8 is a depth–density profile derived from these data.

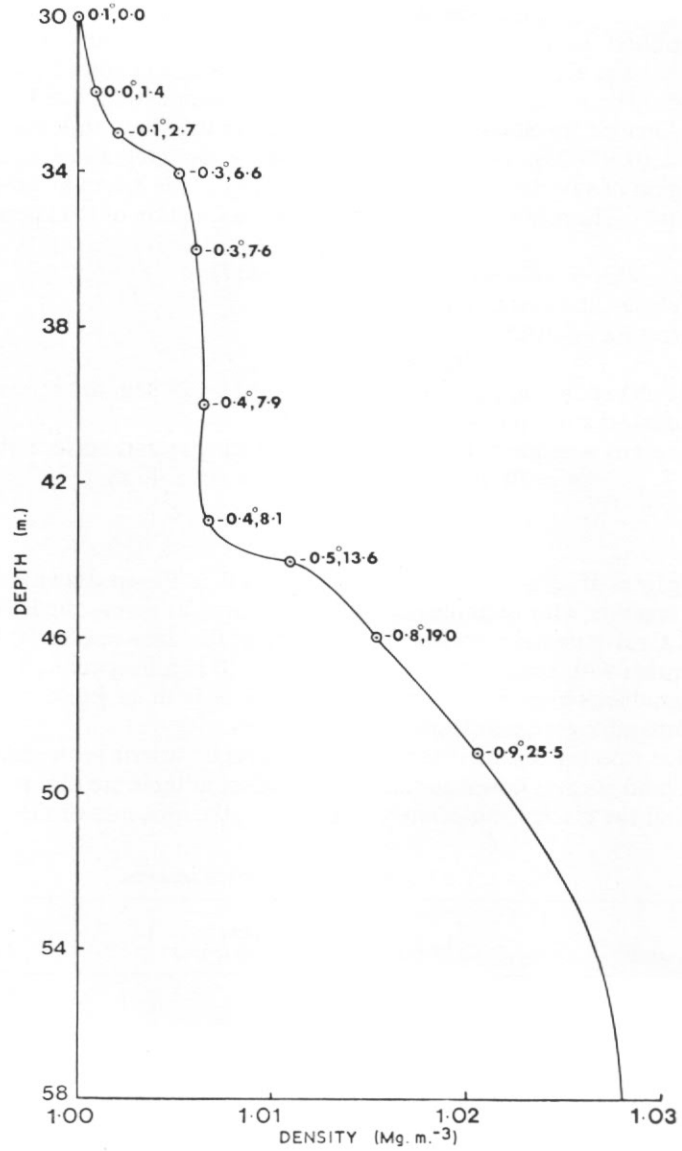

Fig. 8. Depth–density profile of water in a tidal lake in lat. 70°52′S., long. 68°20′W. The figures against the curve indicate temperature (°C) and salinity (parts per thousand).

The observations indicate that the lake is connected to the sea-water beneath the ice shelf.

By assuming hydrostatic equilibrium of the lake with free sea-water, the observed lake mean surface level was reduced to a salt-water equivalent sea-level and the reduced value was used as datum for the level profile. Fortunately, the profile ran close to a radio echo-sounded ice-thickness profile (personal communication from C. W. M. Swithinbank), allowing a comparison between surface elevation and total ice thickness. The comparison gave a mean density for the ice shelf of 0·911 Mg. m.$^{-3}$.

Since no elevations were measured outside the surface-melt area of the ice shelf, an approxi-

mate mean density for this area was derived following the method used by Renner (1969) for the Larsen Ice Shelf. Renner assumed a probable depth–density curve interpolated between observed values for the Ross Ice Shelf (Crary, 1961; Crary and others, 1962) and Skelton Inlet (Crary, 1966). The observed surface densities have been extrapolated on a curve similar to the Ross and Skelton Ice Shelf curves and it is found that the firn layer should reach the density of pure ice (0·917 Mg. m.$^{-3}$) at a depth of 40 m. By integrating the area beneath this curve over the region of variable density the mean density of the layer above 40 m. is estimated to be 0·817 Mg. m.$^{-3}$. The mean ice-shelf density is thus a function of thickness and is expressed by

$$H\bar{\rho}_i = (H-40)\times 0{\cdot}917+(40\times 0{\cdot}817),$$

where H is ice thickness and $\bar{\rho}_i$ is mean ice density.

By assuming hydrostatic equilibrium,

$$H\bar{\rho}_i = (H-h)\times \rho_w,$$

where h is surface elevation and ρ_w is sea-water density (1·028 Mg. m.$^{-3}$), assuming a salinity of 35 parts per thousand and a temperature of −1·7° C.

Eliminating $\bar{\rho}_i$, there is a relation between ice-shelf thickness and surface elevation:

$$h = (0{\cdot}108\times H)+3{\cdot}89 \text{ m. for } H \geqslant 40 \text{ m.}$$

Ice Thickness

A map showing lines of equal ice thickness or isopachs (Fig. 9) was drawn from data reported by Smith (1972) together with unpublished radio-echo profiles across the ice shelf at both the Carse Point and Coal Nunatak profiles. The density of the data was variable but it enabled isopachs to be drawn with reasonable confidence. Fig. 10 is a longitudinal section of the ice shelf. Thickness gradients over the first 80 km. inland from both ice fronts are given in Table I together with comparable gradients from other ice shelves.

A number of ice streams can be detected in the isopach pattern in the form of tongues of thicker ice where land glaciers flow into the ice shelf. Most notable are the streams from Goodenough Glacier and the glacier immediately to its north, the influence of Goodenough Glacier

Table I. Thickness gradients of ice shelves

Ice shelf	*Thickness gradient* (m./100 km. from ice front)	*Source*
George VI Ice Shelf (western ice front)	405	
Brunt Ice Shelf	260	Thomas and Coslett (1970)
Larsen Ice Shelf	160	Swithinbank (1968)
Ross Ice Shelf	110	Zumberge (1971)
George VI Ice Shelf (northern ice front)	70	
Amery Ice Shelf	30	Budd (1966)

extending right across the sound to Two Step Cliffs. Heavy crevassing on Goodenough Glacier seems to confirm that the glacier is fairly active. The area of thinner ice in lat. 72°15′S. is on the down-stream side of Buttress Nunataks. It could be caused by ice streams from Palmer Land being deflected around the nunataks and thus largely by-passing the area immediately down-stream of the obstruction. Farther down-stream, the ice streams merge and restore the ice shelf to its former thickness. Between Goodenough Glacier and Ablation Point, the ice shelf is generally thicker on its eastern side, reflecting large ice discharges from Ryder Glacier and its neighbours. Uranus Glacier on the western side of the sound has a small area of thickening where it flows into the ice shelf. The cause of the area of thin ice adjacent to Succession

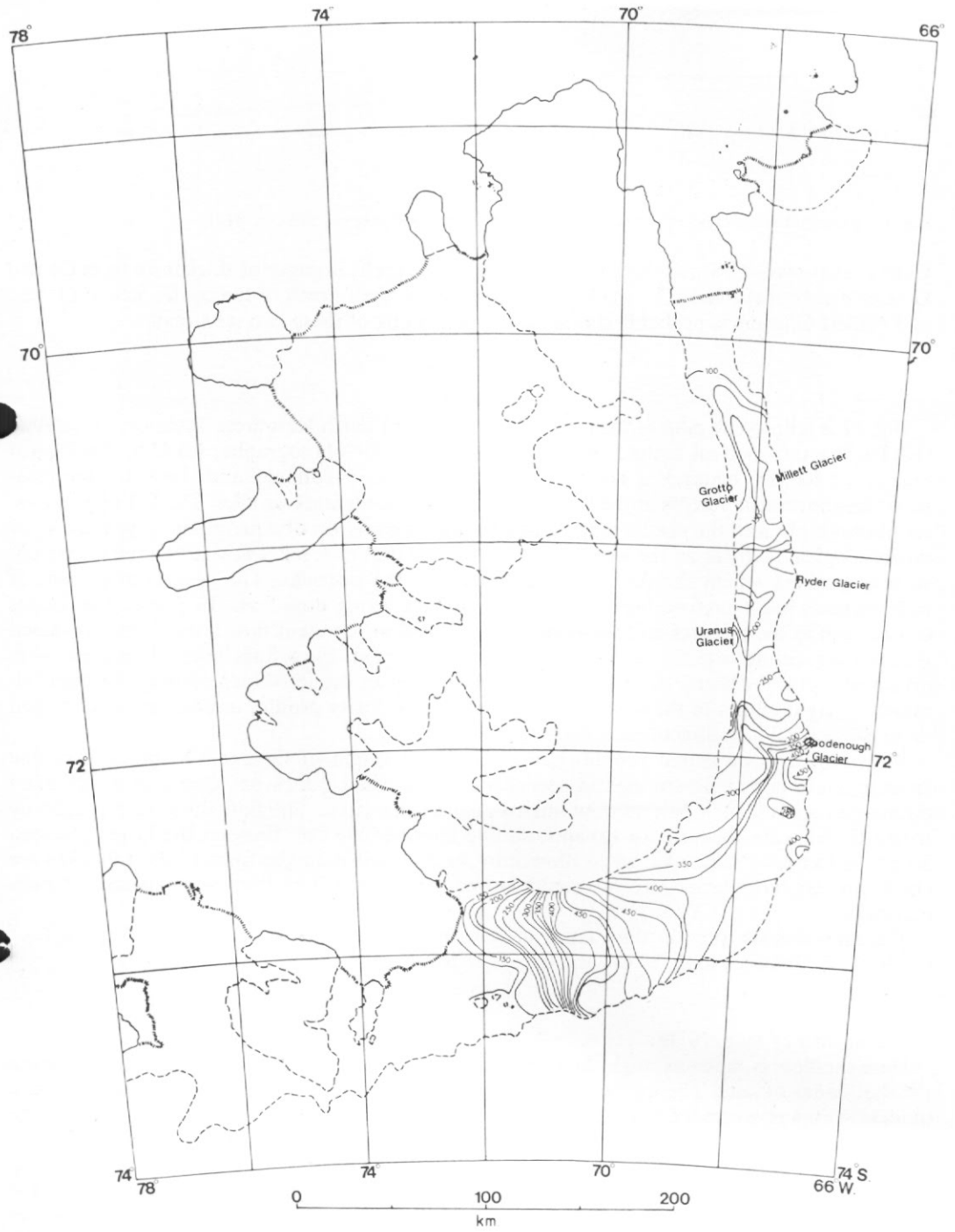

Fig. 9 Ice-thickness isopleths for George VI Ice Shelf.

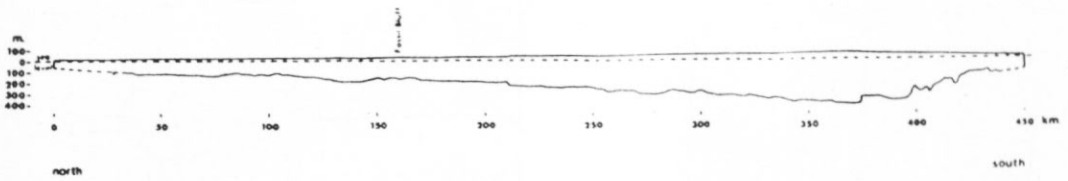

Fig. 10. Longitudinal section of George VI Ice Shelf (after Swithinbank, 1968, p. 410).

Cliffs is unknown. Towards the northern end of the ice shelf, a tongue of thicker ice from Grotto Glacier can be identified. The thicker centre of the ice shelf north of the confluence of Grotto and Millett Glaciers is probably due simply to a meeting of these two ice streams.

Flow Lines

Fig. 11 is a flow-line map of the ice shelf based on: (a) Earth Resources Technology Satellite (ERTS-1) multi-spectral scanner imagery; (b) oblique air photographs; (c) U.S. Geological Survey 1 : 500,000 Antarctica sketch map, Ellsworth Land–Palmer Land sheet; (d) the measured ice-movement vectors at the Carse Point and Coal Nunatak profiles. The ERTS pictures, air photographs and the sketch map, which is based mainly on oblique photographs, all show morphological features on the ice shelf. It is assumed that melt lakes flow along the maximum surface gradient which should be at right-angles to the isopachs. The general alignment of melt features has therefore been interpreted as being along flow lines. In places, low ridges can be seen in the pictures and these are also believed to represent flow lines. Some crevassed glacier tongues indicate the direction of glacier movement. Flow lines other than these were drawn along well-defined ice streams that can be seen in the ice-thickness map, or approximately at right-angles to the isopachs. The measured velocity profiles in both cases confirmed these conjectural flow directions.

With only two measured profiles along the whole length of George VI Sound, flow-line spacing could not be determined in accordance with classical flow-net theory in which mass discharge between each pair of flow lines would be the same. The flow lines were spaced by trying to delineate separate ice streams, adding intermediate flow lines on the larger glaciers. South of Buttress Nunataks, where flow into the ice shelf is in the form of an unbroken ice sheet, no separate glacier streams could be recognized and flow lines were spaced unsystematically.

The map reveals three distinct areas of flow in the sound: west of long. 70°W.; north of lat. 70°45′S.; between long. 70°W. and lat. 70°45′S.

The area west of long. 70°W.

Here the flow is much as might be expected for an area of floating ice constrained between parallel flanks of land. The ice feeding the ice shelf appears to flow at right-angles to the coast, quickly swinging westward towards the ice front. Evidently, most of the flow comes from the Antarctic mainland to the south, since the catchment area to the north is represented only by a narrow peninsula between Bach Ice Shelf and George VI Sound. A group of ice rises in the vicinity of the Eklund Islands appears to block westward flow over the southern part of the ice shelf, causing flow lines to converge into the area north of the blockage. Disturbances extend down-stream from the ice rises, and patches of open sea can sometimes be seen in the summer.

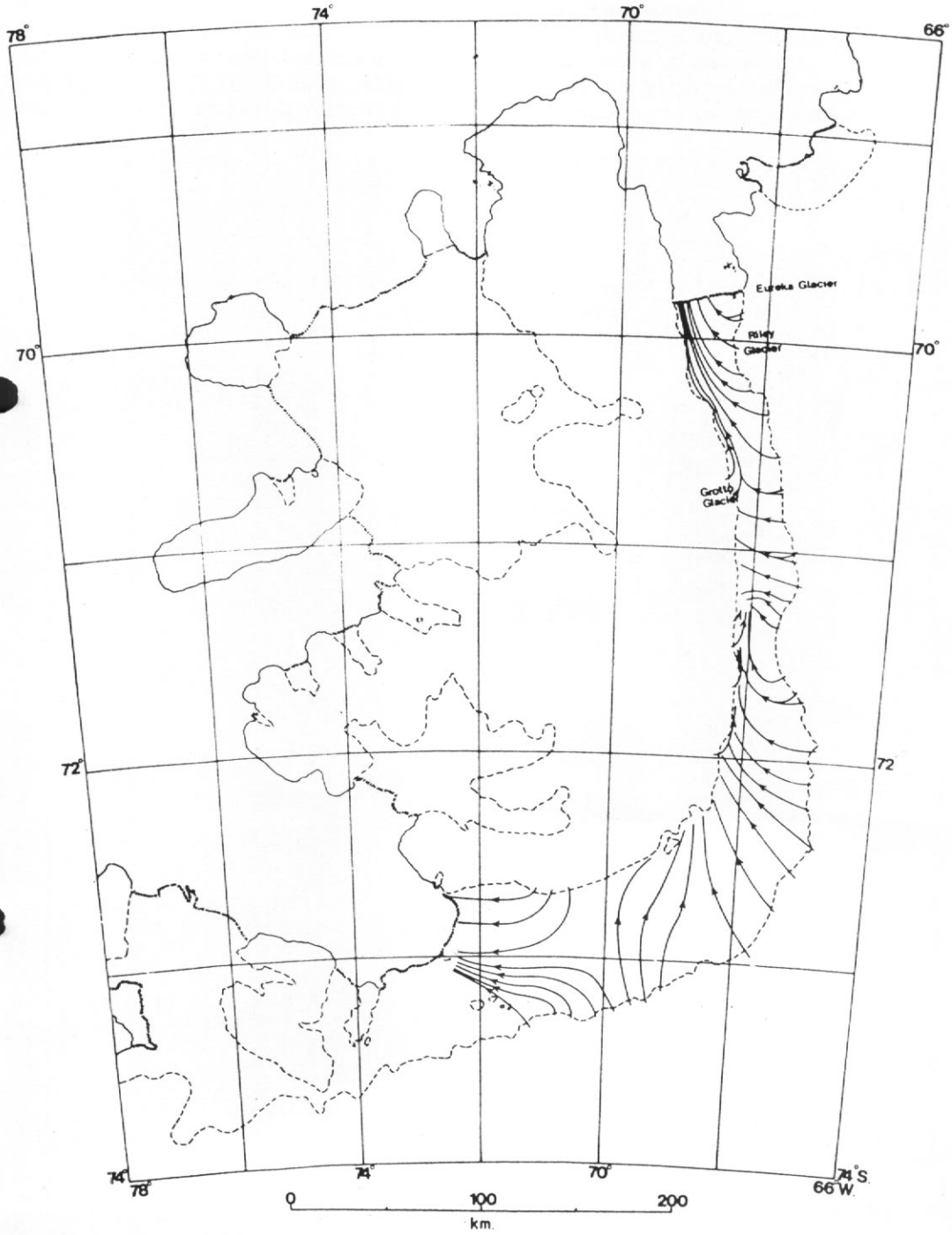

Fig. 11. Flow-line map of George VI Ice Shelf.

The area north of lat. 70°45′S.

The major part of the input here is from the eastern side of the sound. Grotto Glacier is the only glacier flowing from Alexander Island which exhibits any conspicuous signs of activity. A low ridge that indicates the southern margin of ice from Grotto Glacier runs eastward from Ablation Point, turns quickly north and disappears after about 10 km. The much greater input from the east causes a bunching of flow lines on the western side of the ice shelf adjacent

Fig. 12. Satellite view of George VI Ice Shelf between lat. 60°40′ and 71°35′S. The largest ice-free area is the Ablation Point massif. The alignment of melt pools shows the direction of ice movement. Earth Resources Technology Satellite (ERTS-1), scene No. 1170–12251, taken from an altitude of 937 km. on 9 January 1973. The sides of the picture are aligned 35° east of north. (Photograph by the United States National Aeronautics and Space Administration.)

to Alexander Island. An air photograph confirms the almost westerly flow from Riley Glacier and the southern side of Eureka Glacier. While there are no ice-thickness data for the northern part of the ice shelf, the trend of the 100 m. isopach in this area suggests that the ice front is thickest on its western side. Since bunching of flow lines indicates a greater mass discharge per unit width of the ice shelf, increased velocities or thicker ice can be expected.

The area between long. 70°W. and lat. 70°45′S.

The middle section of the ice shelf contrasts with the areas to the north and south. The flow lines appear to be almost completely unaffected by glaciers discharging from Alexander Island. A series of large glaciers from Palmer Land dominates the pattern. The flow pattern shown in this area is based almost entirely on the melt-channel configuration seen in the ERTS pictures (Fig. 12). The movement throughout the area is across the sound, almost directly towards Alexander Island. Ice streams from Palmer Land meet no resistance from opposing glaciers and so are not deflected from their predominantly westerly course. An almost continuous line of pressure ridges along the western margin of the ice shelf in this area supports the evidence of cross flow.

We are faced with the paradox of a 200 m. thick ice shelf flowing towards an immovable mountain range. What happens to the ice when it meets the coast? A possible explanation is suggested by the measurements of bottom flux.

Bottom Flux

The bottom flux of ice shelves is known to be a significant factor in their mass balance. The method of Thomas and Coslett (1970) has been used to calculate bottom-flux rates for George VI Ice Shelf.

Assuming steady-state and using the principle of continuity along a flow line with the ice in hydrostatic equilibrium, Thomas (1972) derived:

$$\dot{A}_s = \rho_w\{Z_b\dot{\epsilon}_z - u\tan\beta\} - \dot{A}_b,$$

where $\dot{A}$ is accumulation rate expressed as mass per unit area (positive $\dot{A}_b$ is bottom freezing rate); u is ice-shelf velocity along the flow line (assumed to be independent of z); $\dot{\epsilon}_z$ is strain-rate (assuming that $\dot{\epsilon}_z = -(\dot{\epsilon}_x + \dot{\epsilon}_y)$ and is independent of z); Z_b is the bottom elevation; ρ_w is density of sea-water (assumed constant); β is bottom slope of the ice shelf (positive for thinning towards the ice front). Suffixes s and b refer to surface and bottom, respectively. The x-axis lies along the flow line at sea-level; the z-axis is upward.

The accumulation rate ($\dot{A}_s$) includes a correction for the compaction of the firn layer. Ice-shelf velocity along the flow line (u) is the measured survey marker velocity. The sea-water density (ρ_w) is assumed to be 1·028 Mg. m.$^{-3}$.

The tangent of the bottom slope (β) is derived from the expression $\tan\beta = -\dfrac{dH}{dx} + \dfrac{dh}{dx}$. As described earlier, the ice thickness (H) and surface elevation (h) are empirically related by the expression $h = 0{\cdot}108H + 3{\cdot}89$ for the areas of the ice shelf that are free of surface melt. Only H is measured directly; radio echo-sounded thicknesses are available for the relevant areas of the ice shelf. However, the radio echo flight lines generally do not follow glacier flow lines, so the isopachs (Fig. 9) have been used to interpolate thickness gradients dH/dx in the direction of ice flow. The bottom surface elevation (Z_b) is simply $H - h$.

Bottom flux rates have been calculated for 11 points on the Carse Point profile at which the principal strains are known, the other factors in the equation being interpolated to these positions. The error in the flux-rate values is estimated to be $\pm 0{\cdot}12$ Mg. m.$^{-2}$ yr.$^{-1}$. Fig. 13 shows a continuous curve of bottom flux rate along the Carse Point profile.

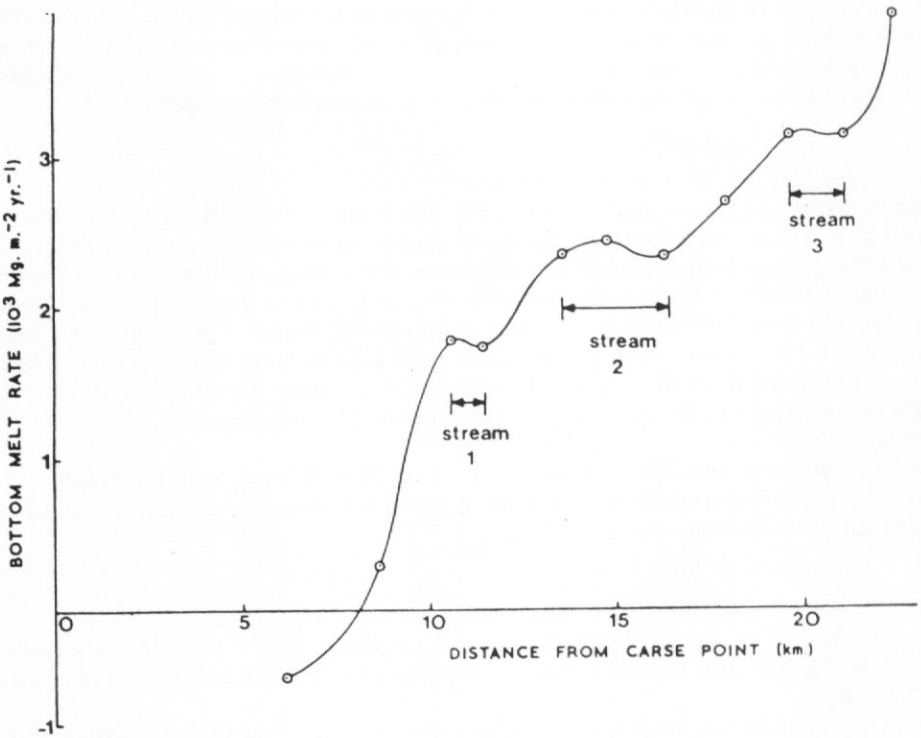

Fig. 13. Bottom-melt rates on the Carse Point profile. The streams are explained in the text.

Bottom flux rates have also been calculated at the two strain-rosette sites on the Coal Nunatak profile. The values are $-0{\cdot}76\pm0{\cdot}2$ Mg. m.$^{-2}$ yr.$^{-1}$ at the centre of the ice shelf and $-1{\cdot}75\pm0{\cdot}3$ Mg. m.$^{-2}$ yr.$^{-1}$ on the western side.

The Significance of Bottom Melting

Let a section of the ice shelf adjacent to Alexander Island be considered, bounded in the north by the Gurney Point–Ablation Point flow line and in the south by a flow line through the Coal Nunatak profile. Interpolation between the measured velocity vectors at each profile enables the probable mean ice velocity for the middle of the ice shelf to be obtained. From Fig. 9 a mean ice thickness for ice flowing into this section can be determined and the mass input to the section can be calculated. No ice can cross a flow line; so the ice must discharge either through the top or bottom surfaces of the ice shelf. Since the eastern coast of Alexander Island consists of an almost continuous line of mountains interspersed with valley glaciers, it is evident that no discharge can take place on to the island. In the absence of mass-balance measurements in this particular area, the evidence of surface melting in summer has been used as a basis for assuming that the surface net balance is zero. If this is true, the principal mass flux must be through the bottom surface of the ice shelf. Knowing the mass input and also the area over which losses can take place, a negative bottom flux (melting) of about 3·5 Mg. m.$^{-2}$ yr.$^{-1}$ would be needed to dispose of all the ice flowing into the area. This figure falls between those obtained at the two measured profiles and it is concluded that bottom melting alone can account for the removal of all the ice flowing towards Alexander Island.

Fig. 13 reveals an unexpected increase in bottom melt rates from east to west on the Carse Point profile. It is apparent from Fig. 11 that the three plateaux of the bottom-melt profile may correlate with ice streams flowing from Chapman Glacier (stream 1), Meiklejohn Glacier (stream 2) and Millett Glacier (stream 3). The melt rate is approximately proportional in each case to the time of travel of an ice particle from the inland boundary of the ice shelf to the Carse Point profile. Since the amount of heat conducted by a body is directly proportional to the temperature gradient in its surface layers, heat flow must decrease as the temperature gradient becomes less steep. Assuming that the amount of heat available from the sea for bottom melting is constant at a given distance from the ice front, it is evident that with the passage of time a decreasing proportion of the heat conducted from the sea must contribute to raising the temperature of the ice shelf. The rest goes to increase the rate of melting.

Fig. 2 shows that the Coal Nunatak profile lies approximately along a flow line. The time taken for an ice particle from the inland boundary of the ice shelf to reach the middle of the profile, where the melt rate is 0·75 Mg. m.$^{-2}$ yr.$^{-1}$, is about the same as the time taken by stream 1 to reach the Carse Point profile where the melt rate is 1·75 Mg. m.$^{-2}$ yr.$^{-1}$. The difference between these values is consistent with the idea that there is a progressive loss of heat available for melting as the sea-water travels further beneath the ice shelf.

Conclusion

The flow-line map (Fig. 11) delineates ice-stream boundaries and reveals that the principal discharge of ice is along George VI Sound. Ice flows unexpectedly across the sound in one area into an ice regime analogous to that of a consuming plate boundary in contemporary plate-tectonic theory. However, instead of being consumed beneath Alexander Island, the ice shelf evidently maintains a positive vertical strain-rate sufficient to balance the rate of bottom melting. The Palmer Land glaciers represent the major source of ice entering the area.

The net mass balance of the bottom surface of the ice shelf was found to be negative in the area of the ice shelf north of about lat. 72°S., melt rates evidently decreasing away from the ice front as less heat remains available in the sea for melting. The Carse Point bottom-melt profile suggests that observing a series of bottom flux rates across the direction of flow might offer a new and relatively simple method of detecting the ice streams in an ice shelf. A series of bottom-flux values measured along an ice stream would give a flux rate versus elapsed time curve, from which the basal temperature of the ice at the point where it flowed off the land on to the sea might be inferred. The profile of bottom flux rates suggests that bottom freezing may occur in the early stages after an ice stream leaves the land.

It is concluded that bottom melting alone can maintain equilibrium against the westward advance of ice towards Alexander Island. Considerable interpolation has been necessary because no data were available between the two measured profiles. In order to test this hypothesis it is suggested that measurements of surface mass balance, ice velocity and strain-rates should now be made in the central section so that actual bottom-flux rates can be calculated for this fascinating area.

Acknowledgements

We wish to thank the many people who helped with the collection of field data. Our particular thanks go to Dr. C. Swithinbank for his helpful guidance during the preparation of this paper.

MS. received 3 January 1975

REFERENCES

BUDD, W. 1966. The dynamics of the Amery Ice Shelf. *J. Glaciol.*, **6**, No. 45, 335–58.

CRARY, A. P. 1961. Glaciological studies at Little America station, Antarctica, 1957 and 1958. *IGY glaciol. Rep. Ser.*, No. 5, 197 pp.

————. 1966. Mechanism for fiord formation indicated by studies of an ice-covered inlet. *Geol. Soc. Am. Bull.*, **77**, No. 9, 911–29.

————., ROBINSON, E. S., BENNETT, H. F. *and* W. W. BOYD. 1962. Glaciological studies of the Ross Ice Shelf, Antarctica, 1957–1960. *IGY glaciol. Rep. Ser.*, No. 6, 193 pp.

RENNER, R. G. B. 1969. Surface elevations on the Larsen Ice Shelf. *British Antarctic Survey Bulletin*, No. 19, 1–8.

SMITH, B. M. E. 1972. Airborne radio echo sounding of glaciers in the Antarctic Peninsula. *British Antarctic Survey Scientific Reports*, No. 72, 11 pp.

SWITHINBANK, C. W. M. 1958. Glaciology. I. The movement of the ice shelf at Maudheim. *Norw.-Br.-Swed. Antarct. Exped., Scient. Results*, **3C**, 77–96.

————. 1968. Radio echo sounding of Antarctic glaciers from light aircraft. *Gen. Assembly int. Un. Geod. Geophys., Berne, 1967. Int. Assoc. sci. Hydrol.*, 405–14. [IASH Publication No. 79.]

THOMAS, R. H. 1970. Survey on moving ice. *Surv. Rev.*, **20**, No. 157, 322–38.

————. 1972. *The dynamics of ice shelves*. Ph.D. thesis, University of Cambridge, 143 pp. [Unpublished.]

————. *and* P. H. COSLETT. 1970. Bottom melting of ice shelves and the mass balance of Antarctica. *Nature, Lond.*, **228**, No. 5266, 47–49.

WAGER, A. C. 1972. Flooding of the ice shelf in George VI Sound. *British Antarctic Survey Bulletin*, No. 28, 71–74.

ZUMBERGE, J. H. 1971. Ross Ice Shelf Project. *Antarct. Jnl U.S.*, **6**, No. 6, 258–63.

————., GIOVINETTO, M., KEHLE, R. *and* J. REID. 1960. Deformation of the Ross Ice Shelf, near the Bay of Whales, Antarctica. *IGY glaciol. Rep. Ser.*, No. 3, 148 pp.